

An Expeditious Spatial Mean Radiant Temperature Mapping Framework using Visual SLAM and Semantic Segmentation

Wei Liang, Yiting Zhang, Ji Zhang, Erica Cochran Hameen
 Carnegie Mellon University
 5000 Forbes Ave, Pittsburgh, Pennsylvania, USA
 {weiliang, yitingzh, zhangji, ericac}@andrew.cmu.edu

Abstract

Ensuring thermal comfort is essential for the well-being and productivity of individuals in built environments. Of the various thermal comfort indicators, the mean radiant temperature (MRT) is very challenging to measure. Most common measurement methodologies are time-consuming and not user-friendly. To address this issue, this paper proposes a novel MRT measurement framework that uses visual simultaneous localization and mapping (SLAM) and semantic segmentation techniques. The proposed approach follows the rule of thumb of the traditional MRT calculation method using surface temperature and view factors. However, it employs visual SLAM and creates a 3D thermal point cloud with enriched surface temperature information. The framework then implements Grounded SAM, a new object detection and segmentation tool to extract features with distinct temperature profiles on building surfaces. The detailed segmentation of thermal features not only reduces potential errors in the calculation of the MRT but also provides an efficient reconstruction of the spatial MRT distribution in the indoor environment. We also validate the calculation results with the reference measurement methodology. This data-driven framework offers faster and more efficient MRT measurements and spatial mapping than conventional methods. It can enable the direct engagement of researchers and practitioners in MRT measurements and contribute to research on thermal comfort and radiant cooling and heating systems.

1. Introduction

Thermal comfort is defined as “the condition of mind which expresses satisfaction with the thermal environment and is assessed by subjective evaluation” [3]. The evaluation of thermal comfort involves physical measurements and subjective factors. Among these measurements, mean radiant temperature (MRT) represents the short- and long-wave ra-

diant heat fluxes reaching the human body. MRT converts radiant heat exchange between the occupant and heterogeneous surrounding surfaces to a similar process between the human body and a uniform enclosure. Deviated MRT can cause thermal discomfort even if the local air temperature of the occupants is acceptable [6].

Assessing MRT is challenging due to its geometric complexity [8] and the peculiarities of the instruments [6]. Most MRT measuring methods, regulated in the ISO 7726 standard [2], are time-consuming, labor-intensive, and require high expertise to handle instruments and perform calculations. Therefore, the MRT assessment is limited to individual measurements due to instrument and technique restrictions. As the **first contribution** of this paper, we proposed a novel data-driven MRT measurement approach using visual simultaneous localization and mapping (SLAM) and semantic segmentation techniques, enabling efficient MRT data collection.

In addition, previous frameworks for spatial MRT rely on either sophisticated simulation software [4, 7], domain knowledge [17], and advanced sensors [5] to extract features. The **second contribution** of this paper is to provide an end-to-end framework using a low-cost camera array and semantic segmentations to extract features automatically. The block diagram of the proposed framework is shown in Fig. 1. The GitHub repository will be published later.

2. Method

2.1. Camera Set Design and Thermal Calibration

The camera array comprises a thermal infrared (TIR) camera, an RGB-D camera, and a tracking camera. The TIR camera used in this study is the FLIR Lepton 3.5 [1]. Previous distance calibration results[11] have suggested that the FLIR Lepton 3.5 provides precise and consistent distance measurements within the range of 0.8 to two meters. The camera set also includes Intel® RealSense™ Tracking Camera T265 in tandem with the Intel® RealSense™ Depth Camera D435i. All three cameras are rigidly cou-

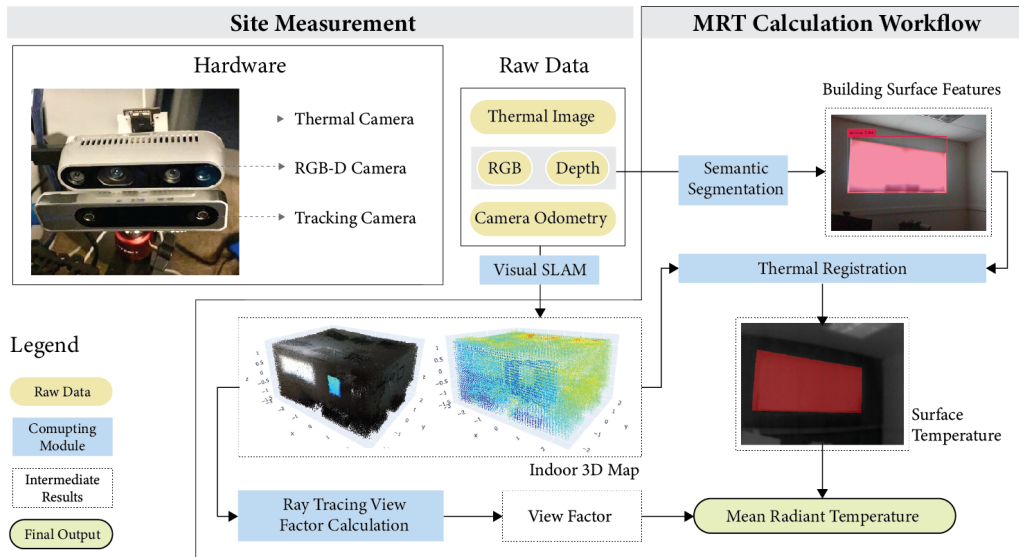


Figure 1. The block diagram of the proposed framework.

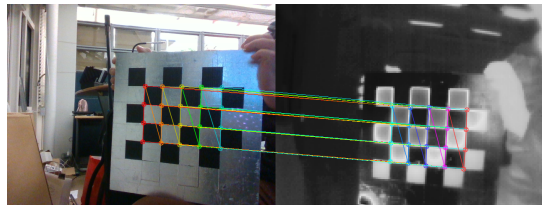


Figure 2. Left: RGB image. Right: thermal image.

pled together, spatially aligned in a 3D-printed frame, and mounted on the top of a mobile sensing platform, as shown in Fig. 1.

The homogeneous transformation between the RGB-D camera and tracking can be found in its official guideline [16]. However, stereo vision calibration between the RGB-D and TIR cameras is still needed for other modules in the proposed framework. Traditional calibration targets may not result in distinct geometric patterns visible in infrared images. Therefore, a specially designed checkerboard made of silver aluminum foil and black polyethylene material ensures conspicuous contrast in both visible and thermal ranges. As illustrated in Fig. 2, when heated by a radiator, the aluminum foil squares absorb additional infrared energy and appear dark, while the polyethylene squares emit more infrared energy and appear bright in the thermal image. The mean re-projection error (MRE) of 80 image pairs is 0.80 pixels. Similar TIR camera calibration approaches can be found in [11, 12].

2.2. Visual SLAM and Thermal Data Fusion

The proposed framework implements a visual simultaneous localization and mapping (vSLAM) system, enabling the camera array to incrementally build a map and localize itself in an unknown indoor environment. The vSLAM approach this framework applies is real-time appearance-based mapping (RTAB-Map), given its loop closure detection feature and efficient memory management [10].

Since the thermal infrared images are insufficient in frequency, field of view, and resolution, the thermal data fusion is implemented after the real-time measurement. At each synchronized timestamp t , the proposed framework maps thermal images with depth images and creates a local point cloud with temperature information. After that, the thermal point cloud is transformed to the world coordinates using the camera odometry at the current timestep. A K-D Tree-based iterative closest point algorithm [15] aligns and merges local thermal point clouds to a 3D indoor thermal map. Fig. 3 shows the RGB point cloud retrieved during the vSLAM process and the thermal point cloud retrieved offline.

2.3. Semantic Segmentation for Thermal Features

The primary reason for potential significant inaccuracies in MRT calculation using surface temperatures and view factors is that building envelopes in built environments have non-uniform surface temperatures. Walls, floors, ceilings, and other surfaces may contain different features, such as windows, paintings, lighting, skylights, and other building components, leading to different temperature profiles across different surface areas. Therefore, we must detect and

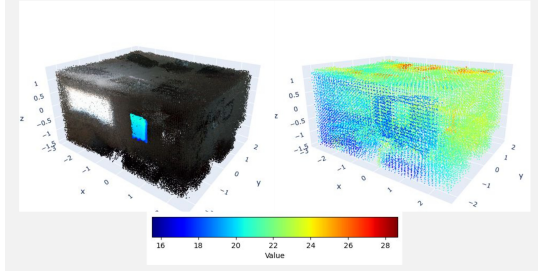


Figure 3. Left: RGB point cloud with a registered thermal feature, painting. Right: thermal point cloud.

segment the building surface features from the main surface areas. To achieve this goal, we implement Grounded SAM [14], which uses Grounding DINO [13] as an open-set object detector to combine with the segment anything model (SAM) [9]. It provides open-vocabulary object detection, enabling the recognition of various building surface features that are not prevalent in most common datasets.

When vSLAM processes sequential frames to generate a point cloud, each instance segmentation result is assigned a label or multiple labels over time based on outputs from the object detector. These labels correspond to different building surface features identified in the point cloud. Each feature is uniquely identified, and then "votes" for its label are based on the frequency of each label it has been assigned. The label that receives the most votes is selected as the final label for that feature. This approach ensures consistency and stability in the segmentation results by favoring the most common labels over time.

After segmentation, each feature's temperature profile is re-projected to the thermal point cloud. On the left of Fig. 3, the temperature profile of the feature "painting" on the wall is re-projected to the point cloud for view factor calculation.

An example of thermal feature segmentation is shown in Fig. 4. We defined a label named "recessed lighting" to extract the related features on the ceiling. Grounded SAM detected and segmented this object type successfully. Using depth images that share the same frame as the RGB image, we can register the feature on the corresponding thermal image, where the recessed lighting exhibits a lighter color than its surrounding ceiling tile, indicating that it has a different temperature profile.

2.4. Mean Radiant Temperature Calculation

The proposed framework for MRT measurement is based on the calculation approach from the temperature of the surrounding surfaces and the view factors between the observation point and the surrounding surfaces per ISO 7726 [2]. The following Eq. (1) is used:



Figure 4. Detection and segmentation of ceiling feature "recessed lighting" on RGB image, and registration on the thermal image at approximately the same timestamp.

$$\bar{T}_r = \sqrt[4]{\frac{\sum_{i=1}^n F_i \cdot T_i^4}{\sum_{i=1}^n F_i}}, \quad (1)$$

Where \bar{T}_r is the mean radiant temperature in kelvins, T_i is the surface temperature of surface or feature i in kelvins, and F_i is the view factor between the observation point and surface or feature i .

In the MRT calculation process, view factor calculation plays an indispensable role. We implement the Monte Carlo-based ray tracing algorithm to estimate view factors. A large number of rays are simulated, and the view factor is calculated by the proportion of rays intersecting with surfaces and features.

The mean radiant temperature calculation algorithm is provided in Algorithm 1.

Algorithm 1 Mean Radiant Temperature Calculation

- 1: **for** Each building envelope i **do**
 - 2: Retrieve surface plane and corners
 - 3: Calculate the initial view factor of the envelope F_i
 - 4: **if** Thermal features are found **then**
 - 5: **for** Each thermal feature j **do**
 - 6: Retrieve surface corners
 - 7: Calculate the view factor of the feature $F_{i,j}$
 - 8: Compute feature surface temperature $T_{i,j}$
 - 9: Correct the view factor of the envelope:

$$F_i = F_i - F_{i,j}$$
 - 10: **end for**
 - 11: **end if**
 - 12: Compute subtracted building envelope surface temperature T_i
 - 13: **end for**
 - 14: Calculate MRT using Eq. (1)
-

3. Results and Discussions

The experiment was conducted on February 6th, 2024, in an enclosed office room in Pittsburgh, Pennsylvania, USA. The outdoor air temperature is about $1.1^\circ C$. The indoor air setpoint is $21.0^\circ C$. The wall facing east has a window,

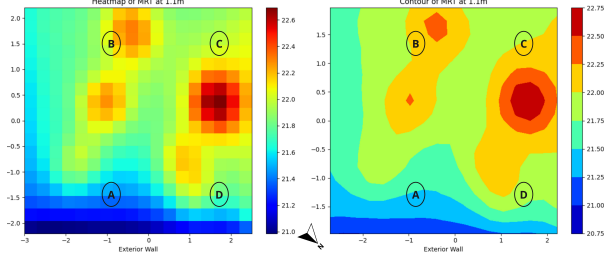


Figure 5. The heatmap and contour representations of the MRT radiant field were reconstructed using the proposed framework. Locations labeled A through D are the measurement points using a black-globe thermometer.

while the remaining three walls are connected to an open office space that shares the same HVAC system as the test environment. The handheld visual SLAM procedure took approximately 343 seconds to complete. Due to the short duration, we assume no temporal variations in MRT for this scenario.

3.1. Spatial Field Mapping of MRT

To generate the spatial field mapping of the MRT during the experiment, a 20×20 mesh grid is applied to the indoor environment, and the MRT at each location is calculated using Eq. (1). The height of the MRT measurement is set at 1.1 meters above the floor, which is the height of the head and eyesight of occupants when sitting. As shown in Fig. 5, we can learn that the outdoor air temperature and the location of windows impact the spatial distribution of MRT. The area near the exterior wall exhibits lower MRT. However, a gradient ascent of MRT is in line with the increased directional solar exposure. We can also observe distinct warm zones near location C with a steep temperature gradient, indicating its proximity to heat-generating features, namely the recessed lights. In summary, the spatial distribution map of MRT provides more insights into the spatial variation of thermal comfort than individual measurements.

3.2. Results Validation with Reference Method

During the experiment, we also measured MRT using the black-globe thermometer as the reference measurement at four locations. The black-globe thermometer is considered a standard MRT measuring method, but it needs a long response time, and the instrument is bulky. The MRT measured from this reference method is:

$$T_{mrt} = \sqrt[4]{T_g^4 + 0.4 \times 10^8 (T_g - T_a)^4 \sqrt{|T_g - T_a|}}, \quad (2)$$

where T_g is the globe temperature measured by the black-globe thermometer and T_a is the local air temperature. The globe thermometer is placed at 1.1 meters above the floor.

Location	Black-globe	Ours	$\Delta \bar{t}_r (^{\circ}C)$
A	21.8 $^{\circ}C$	21.4 $^{\circ}C$	-0.4
B	21.6 $^{\circ}C$	22.2 $^{\circ}C$	+0.6
C	21.5 $^{\circ}C$	22.0 $^{\circ}C$	+0.5
D	21.1 $^{\circ}C$	21.5 $^{\circ}C$	+0.4

Table 1. Comparison between the MRT measurements by the proposed framework and the reference method.

Note that each measurement takes 15 minutes for the globe thermometer to respond to the surroundings.

As shown in Tab. 1, the reference observations were conducted across four distinct locations, labeled A through D in Fig. 5. The data reveal a slight variance between the two sets of measurements, with the differences of MRT measurements in Celsius (t_r) ranging from -0.4 to +0.6 $^{\circ}C$. Specifically, locations B and C exhibited higher MRT values as measured by our method compared to the reference, indicating a potential overestimation by our framework in these instances. The MRT measurement deviations at all locations comply with the range of the required accuracy ($\pm 2^{\circ}C$) specified by ISO 7726 [2], though not within the desired range ($\pm 0.2^{\circ}C$). Since each measurement of the reference method possesses a long response time, the temporal differences or methodological nuances may contribute to the observed variances.

3.3. Limitations and Future Work

Several limitations are involved in the proposed framework and experiment presented. Firstly, vSLAM can drift. Loop closure may not be guaranteed when the framework is applied to a larger indoor environment. Future improvements may involve using 3D-lidar and implementing pose graph optimization. Another limitation is that the experiment only compares the proposed framework with the black-globe method, which is coupled with a temporal discrepancy in the readings due to the long response time inherent to the black-globe method. Future work will broaden the comparative analysis with more standard MRT measurement methodologies, including the contact thermometer measurement approach and the calculation methods based on surface areas.

4. Conclusion

This paper proposed an efficient data-driven mean radiant temperature measuring method using an RGB-D-TIR-Tracking camera array, visual SLAM, and semantic segmentation. The proposed framework detects and segments distinct building envelope surfaces and features in the built environment. It then calculates the corresponding view factors from the point of view using the Monte Carlo-based ray tracing method. The framework can calculate the MRT

at any location in the indoor environment and generate a spatial distribution of MRT in an indoor environment based on detailed surface temperature information from the space. The proposed method can be used for research on thermal comfort and radiant systems and serve as part of the digital twin of a built environment for monitoring indoor environmental quality.

References

- [1] Lepton LWIR Micro Thermal Camera Module | Teledyne FLIR. <https://www.flir.com/products/lepton?vertical=microcam&segment=oem>, 2024. Accessed: 2024-03-06. **1**
- [2] ISO 7726:1998(E). Ergonomics of the thermal environment — instruments for measuring physical quantities. Standard, International Organization for Standardization, Geneva, CH, 1998. **1, 3, 4**
- [3] ANSI/ASHRAE. ANSI/ASHRAE Standard 55-2023: Thermal Environmental Conditions for Human Occupancy. Standard, American Society of Heating, Refrigerating and Air-Conditioning Engineers, Atlanta, GA, USA, 2023. **1**
- [4] Dorit Aviv, Nicholas Houchois, and Forrest Meggers. Thermal reality capture merging heat-sensing with 3d scanning and modeling to characterize the thermal environment. In *39th Annual Conference of the Association for Computer Aided Design in Architecture: Ubiquity and Autonomy, ACADIA 2019*, pages 338–345. ACADIA, 2019. **1**
- [5] Dorit Aviv, Julie Gros, Hayder Alsaad, Eric Teitelbaum, Conrad Voelker, Jovan Pantelic, and Forrest Meggers. A data-driven ray tracing simulation for mean radiant temperature and spatial variations in the indoor radiant field with experimental validation. *Energy and Buildings*, 254:111585, 2022. **1**
- [6] Francesca Romana d’Ambrosio Alfano, Marco Dell’Isola, Boris Igor Palella, Giuseppe Riccio, and Aldo Russi. On the measurement of the mean radiant temperature and its influence on the indoor thermal environment assessment. *Build. Environ.*, 63:79–88, 2013. **1**
- [7] Miaomiao Hou, Dorit Aviv, Arnab Chatterjee, Eric Teitelbaum, Mohamad Rida, Forrest Meggers, and Dolaana Khovalyg. Resolving indoor shortwave and longwave human body irradiance variations for mean radiant temperature and local thermal comfort. *Energy Build.*, 301:113581, 2023. **1**
- [8] Noémi Kántor and János Unger. The most problematic variable in the course of human-biometeorological comfort assessment — the mean radiant temperature. *Central European Journal of Geosciences*, 3(1):90–100, 2011. **1**
- [9] Alexander Kirillov, Eric Mintun, Nikhila Ravi, Hanzi Mao, Chloe Rolland, Laura Gustafson, Tete Xiao, Spencer Whitehead, Alexander C. Berg, Wan-Yen Lo, Piotr Dollar, and Ross Girshick. Segment anything. In *Proceedings of the IEEE/CVF International Conference on Computer Vision (ICCV)*, pages 4015–4026, 2023. **3**
- [10] Mathieu Labbé and François Michaud. RTAB-Map as an open-source lidar and visual simultaneous localization and mapping library for large-scale and long-term online operation. *J. Field Robot.*, 36(2):416–446, 2019. **2**
- [11] Da Li, Carol C Menassa, and Vineet R Kamat. Robust non-intrusive interpretation of occupant thermal comfort in built environments with low-cost networked thermal cameras. *Appl. Energy*, 251:113336, 2019. **1, 2**
- [12] Ruixuan Liu, Hengrui Zhang, and Sebastian Scherer. Multiple methods of geometric calibration of thermal camera and a method of extracting thermal calibration feature points. Technical report, Robotics Institute, Carnegie Mellon University, 2018. **2**
- [13] Shilong Liu, Zhaoyang Zeng, Tianhe Ren, Feng Li, Hao Zhang, Jie Yang, Chunyuan Li, Jianwei Yang, Hang Su, Jun Zhu, and Lei Zhang. Grounding dino: Marrying dino with grounded pre-training for open-set object detection, 2023. **3**
- [14] Tianhe Ren, Shilong Liu, Ailing Zeng, Jing Lin, Kunchang Li, He Cao, Jiayu Chen, Xinyu Huang, Yukang Chen, Feng Yan, Zhaoyang Zeng, Hao Zhang, Feng Li, Jie Yang, Hongyang Li, Qing Jiang, and Lei Zhang. Grounded sam: Assembling open-world models for diverse visual tasks, 2024. **3**
- [15] S Rusinkiewicz and M Levoy. Efficient variants of the ICP algorithm. In *Proceedings Third International Conference on 3-D Digital Imaging and Modeling*, pages 145–152. IEEE, 2001. **2**
- [16] Phillip Schmidt, J Scaife, M Harville, S Liman, and A Ahmed. Intel® realsense™ tracking camera t265 and intel® realsense™ depth camera d435-tracking and depth. https://www.intelrealsense.com/wp-content/uploads/2019/11/Intel_RealSense_Tracking_and_Depth_Whitepaper_rev001.pdf, 2019. Accessed: March 26, 2024. **2**
- [17] Eric Teitelbaum, Hongshan Guo, Jake Read, and Forrest Meggers. Mapping comfort with the smart (spherical motion average radiant temperature) sensor. In *Proceedings of Building Simulation*, pages 7–9, 2017. **1**